

# Synthesis and Properties of YbB<sub>2</sub>

M. A. Avila<sup>\*</sup>, S. L. Bud'ko, C. Petrovic<sup>1</sup>, R. A. Ribeiro,  
P. C. Canfield

*Ames Laboratory and Department of Physics and Astronomy  
Iowa State University, Ames, IA 50011*

A. V. Tsvyashchenko, L. N. Fomicheva

*Institute for High Pressure Physics  
RAS, Troitsk, Moscow region, 142092, Russia*

---

## Abstract

We report temperature and field dependent measurements of the magnetic susceptibility, specific heat and resistivity of sintered YbB<sub>2</sub> pellets, prepared via two distinct reaction routes, utilizing different temperatures, pressures and sintering times. Sample behavior is affected by the preparation procedure, as a consequence of different secondary phases, most of which were identified via x-ray diffraction. These experiments show that YbB<sub>2</sub> is a metal with the Yb atoms in or very close to their 3+ state. YbB<sub>2</sub> appears to order anti-ferromagnetically at  $T_N = 5.6 \pm 0.2$  K, which can be considered a relatively high ordering temperature for an ytterbium-based intermetallic compound.

*Key words:* magnetically ordered materials, X-ray diffraction, magnetic measurements, heat capacity, electronic transport

---

## 1 Introduction

With the recent discovery of superconductivity below  $\sim 40$  K in MgB<sub>2</sub>(1), interest has been renewed in the electronic ground state and other physical properties of metal-diborides of the simple hexagonal AlB<sub>2</sub> type structure

---

<sup>\*</sup> Corresponding author

*Email address:* [avila@ameslab.gov](mailto:avila@ameslab.gov) (M. A. Avila).

<sup>1</sup> *Present address:* Brookhaven National Laboratory, Upton, NY 11973

(space group  $P6/mmm$ ), a family which has a large number of members, related to the fact that the metal ions easily deform their electronic clouds in order to fit in between two hexagonal boron rings(2). A common route used to help understand details of the ground state of any given compound is to introduce elemental substitutions in the lattice, and follow the trends of its physical properties as the proportion of the substituting element is increased. Although some successful substitutions have been reported in the particular case of  $MgB_2$ , this compound has so far shown considerable resistance towards admitting foreign elements in its lattice. Thus, a better understanding of physical properties and preparation procedures of isostructural compounds may prove useful.

$YbB_2$ , in particular, has been known as a compound for about 3 decades(3), but presently only crystallographic and chemical characterizations are reported(2; 3). Given the rich variety of interesting electronic, thermodynamic and magnetic properties often displayed by  $Yb$  compounds such as mixed or intermediate valency(4; 5) and heavy fermion behavior(6; 7; 8), plus the considerations described in the previous paragraph, it seemed worthwhile to develop a few growth techniques for  $YbB_2$  and investigate this compound in greater detail.

## 2 Experimental Details

We obtained sintered pellets of  $YbB_2$  by two different synthetic routes. The first route, which we will call “low-pressure synthesis” (LPS), was developed in Ames Laboratory and involved sealing mixtures of both elements in a 6 cm tantalum tube under partial argon atmosphere. The total starting mass was between 1.5 and 2 g, and an excess of  $Yb$  (20%) was introduced to compensate for losses associated with the high vapor pressure of  $Yb$ . Starting reagents were Ames Laboratory  $Yb$  ingots (99.95%) and Eagle-Picher  $^{11}B$  powder (99.95%). For sintering temperatures up to 1200°C the Ta tube was subsequently sealed inside an evacuated quartz ampoule, and this ampoule was heated in a box furnace for the desired temperature and time, after which it was quenched to room temperature by placing the ampoule under running tap water. For sintering temperatures above 1200°C the sealed Ta tube was heated inside a vertical tube furnace with flowing argon atmosphere, and after the desired sintering time was complete the furnace was turned off and allowed to cool to room temperature over several hours. To describe the samples prepared through these LPS procedures we will adopt a notation of the type TTT/HH, where TTT is the sintering temperature in °C and HH is the sintering duration in hours.

The second route was developed in the Institute for High Pressure Physics and used high-temperature, high-pressure synthesis (HPS). Samples were synthe-

sized using the high pressure cell designed by Khvostantsev *et al.*(9). Stoichiometric amounts of elemental ytterbium and boron were placed in the high pressure cell in a NaCl envelope and heated at 6 GPa pressure to 1120°C for 15 minutes (sample 6 GPa) or heated at 8 GPa pressure until melting, then cooled down and crystallized (sample 8 GPa).

Powder X-ray diffraction measurements were made with Scintag and Philips diffractometers using a Cu  $K_{\alpha}$  radiation. A Si powder standard was added to the sample for all runs. The Si lines have been removed from the X-ray diffraction data, leading to apparent gaps in the powder X-ray spectra. Peak positions were compared to those listed in the ICDD-JCPDS database.

Magnetization measurements were made on Quantum Design MPMS systems using the standard operating modes, allowing measurements down to 1.8 K in temperature and up to 55 kOe or 70 kOe in field, depending on the machine. Samples were cooled to 1.8 K under zero applied field, after which the desired measuring field was applied and data taken using 6 cm scan length as the temperature was increased in steps of 0.1-0.25 K at low temperatures, then 1-5 K at higher temperatures. Electrical resistance measurements were performed using these same MPMS systems operated in external device control (EDC) mode, in conjunction with Linear Research LR400/LR700 four-probe ac resistance bridges. Some resistance measurements were also taken on a Quantum Design PPMS system using its own ac resistance bridge option. The electrical contacts were placed on the samples using 4-probe geometry. Pt wires were attached to a sample surface with Epotek H20e silver epoxy, cured at 120°C for  $\sim$  30 minutes. The irregular shape and porosity of the pellets does not allow a reliable estimate of the material's resistivity, so only normalized resistance is presented in this work. Specific Heat measurements were made on the Quantum Design PPMS system with the high-vacuum and specific heat options, allowing measurements down to 1.9 K. The contribution of the grease addenda used to provide thermal contact with the sample was measured separately before each run and discounted from the measurements afterwards.

### 3 Characterization of samples prepared using low-pressure synthesis

#### 3.1 X-Ray Powder Diffraction

The evolution of the YbB<sub>2</sub> sample quality with reaction temperature and time for the LPS samples was followed with X-Ray diffraction measurements, some of which are presented in figure 1 for  $20^{\circ} \leq 2\Theta \leq 42^{\circ}$ . The actual runs were

made between 20° and 90°, but all the necessary information for our analysis is contained in the region shown.

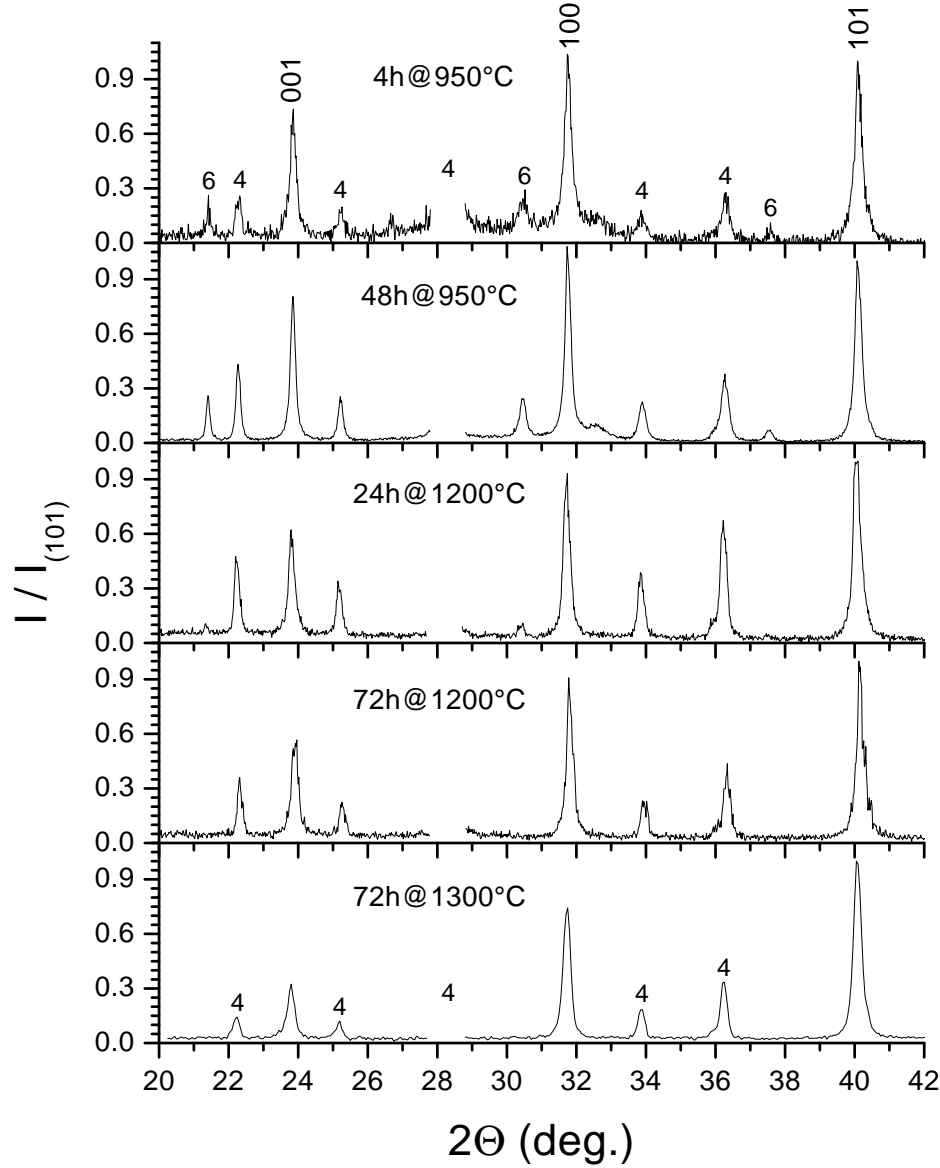


Fig. 1. X-Ray powder diffraction pattern of  $\text{YbB}_2$  from different sinterings. The 3 major peaks are the  $\text{YbB}_2$  reflections in the shown interval (001,100,101), and the data has been normalized by the intensity of the 101 peak. The other labels in the top and bottom graphs mark the peak positions for (4) $\text{YbB}_4$  and (6) $\text{YbB}_6$ . No other compounds are detectable in these samples.

We began by applying a procedure similar to the one we consider ideal for sintering  $\text{MgB}_2$  pellets - 950°C for 4 hours, which results in nearly 100% pure

$\text{MgB}_2$  phase. Sample 950/4 already showed mostly  $\text{YbB}_2$  phase, as can be seen in the top diffractogram of figure 1, where the 3 major peaks belong to the (001), (100) and (101) reflections of  $\text{YbB}_2$ . But clearly visible are sets of peaks attributed to the higher borides  $\text{YbB}_4$  and  $\text{YbB}_6$ , labelled as (4) and (6) respectively. A strong Si reflection centered at  $28.6^\circ$  has been removed from these data. We found no evidence for the presence of  $\text{Yb}_2\text{O}_3$  in these diffractograms, a common magnetic impurity in Yb-based compounds which would manifest as a single peak above noise level centered at  $29.6^\circ$ . There was no clear sign of unreacted Yb reflections either, indicating that the excess Yb introduced in the growth mostly condenses on the internal walls of the Ta tube which, several days after opening, turns into an oxidized powdery layer that peels off easily. It is likely that a small amount of Yb also condenses in the sintered pellet, but not enough to be detectable in the diffractogram as either Yb or  $\text{Yb}_2\text{O}_3$ .

The next diffractogram in fig. 1 is for sample 950/48, which was measured using more extended data acquisition time to reduce noise level and improve resolution. No significant change is seen in the relative heights of the measured peaks for different phases, which would indicate that sintering for longer times at this temperature does not significantly reduce the amount of secondary phases in  $\text{YbB}_2$ .

The third, fourth and fifth diffractograms in fig. 1 show that by increasing temperature and time we are able to progressively reduce the amount of  $\text{YbB}_6$  in the samples. By 1200/72 this compound is fully suppressed. However, even at 1300/72 there is still easily detectable  $\text{YbB}_4$ . Comparing peak heights between different phases is not a reliable method to quantitatively evaluate their proportion, but at a gross level we can state from the X-Ray data that the amount of  $\text{YbB}_4$  is more than 5% and probably less than 30% in the 1300/72 sample. A better estimate is obtained with the analysis of the magnetization data below. The lattice parameters obtained from Rietveld refinement of sample 1300/72 for the  $\text{YbB}_2$  phase are  $a = 3.256(1)\text{\AA}$ ,  $c = 3.735(1)\text{\AA}$ , and for the  $\text{YbB}_4$  phase  $a = 7.071(1)\text{\AA}$ ,  $c = 3.982(1)\text{\AA}$ .

### 3.2 DC Magnetization

The magnetic behavior of the sintered pellets was also measured for the different sintering procedures, and evolved consistently with the trends seen in the X-Ray measurements. Since for both  $\text{YbB}_4$  and  $\text{YbB}_6$  the Yb ions are in (or very close to) their non-magnetic  $2+$  state(10; 11; 12), the effect of these impurities in magnetic measurements is essentially limited to an overestimate of the actual value the  $\text{YbB}_2$  mass, which in turn results in underestimating the effective moment of  $\text{Yb}^{3+}$  in the diboride. Indeed, by fitting the high tempera-

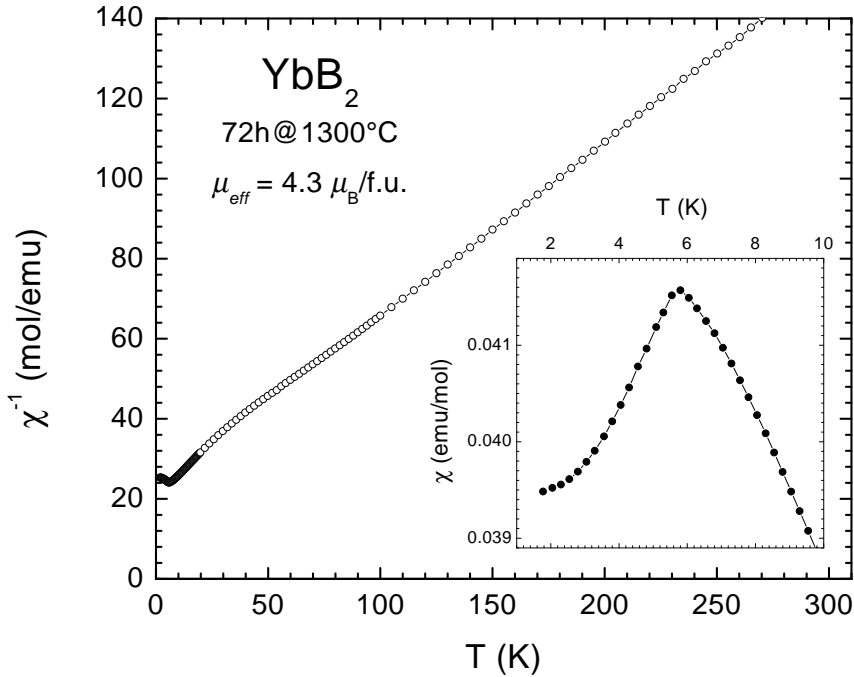


Fig. 2. Temperature dependence of the inverse magnetic susceptibility  $\chi^{-1}(T)$  of a pellet from batch 1300/72, at an applied field of 1 kOe. The inset shows the detail of the anti-ferromagnetic transition below 5.7 K in  $\chi(T)$ .

ture inverse susceptibility we found that  $\mu_{eff}$  increases from  $3.6 \mu_B/YbB_2$  for sample 950/4 to  $4.3 \mu_B/YbB_2$  for sample 1300/72, approaching the expected value of  $4.5 \mu_B/Yb$ . By inverting this analysis, we can estimate that about 9% of the 1300/72 sample is  $YbB_4$ , assuming that it is the primary impurity in this sample as evidenced from the X-Ray pattern. From this point on we will focus on the results from sample 1300/72.

Figure 2 shows the inverse magnetic susceptibility  $\chi^{-1}(T)$  of sample 1300/72 taken in an applied field of  $H = 1$  kOe, with the inset showing a drop in the susceptibility  $\chi(T)$  below 5.7 K, which we associate with anti-ferromagnetic ordering of  $YbB_2$ . Using the criterion of maximum in  $d(\chi T)/dT$ (13) we obtain a somewhat lower value of  $T_N = 5.4 \pm 0.2$  K. In terms of Yb-based intermetallic compounds this is a relatively high ordering temperature. For comparison, Bonville *et al.* had already called attention to the unusually high ordering temperature of 4.2 K in  $YbNiBC$ (14). The high temperature inverse susceptibility is consistent with Curie-Weiss behavior, with  $\theta_p = 49$  K. A clear deviation from linear Curie-Weiss behavior is seen below  $\sim 100$  K, typical of magnetic Yb compounds, and often attributed to crystalline electric field (CEF) effects. The field dependence of this sample's magnetization at  $T = 1.8$  K was also measured, it is essentially linear and featureless in the field range of 0 - 5.5

kOe, reaching a value of  $0.4 \mu_B/\text{YbB}_2$  at the highest field.

### 3.3 Heat Capacity

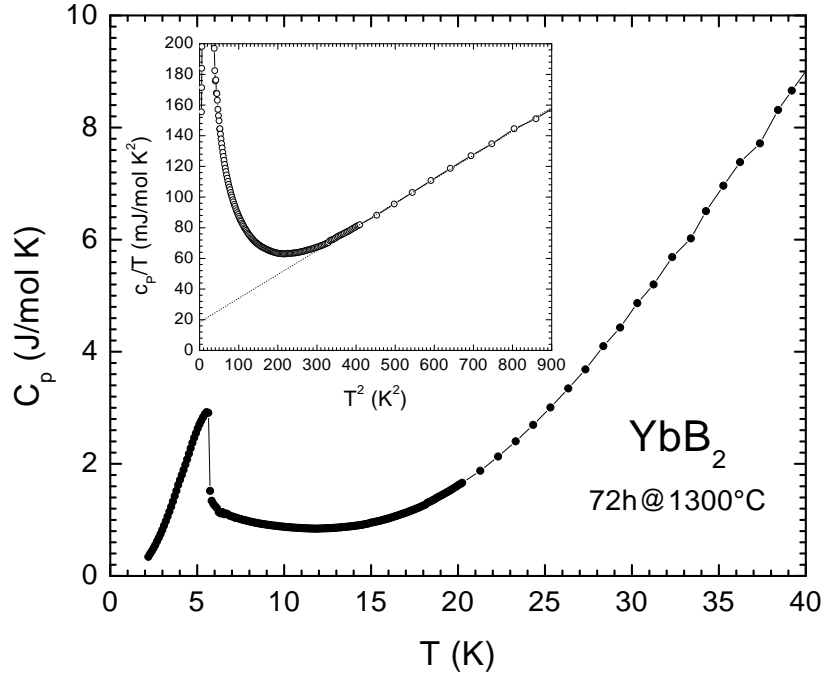


Fig. 3. Temperature dependence of the specific heat of a pellet from batch 1300/72, showing a sharp rise below 5.7 K due to magnetic ordering. The inset shows the  $T^2$  dependence of  $C_p/T$ , where an estimate of  $\gamma = 18 \text{ mJ/mol K}^2$  was obtained by linear fitting of the data between 400 and 900 K $^2$ .

Figure 3 shows zero-field specific heat data of sample 1300/72, taken between 2 K and 40 K. The higher temperature region is dominated by the electronic and lattice contributions, whereas the low temperature data shows a sharp increase in  $C_p$  at 5.7 K due to the anti-ferromagnetic ordering. From these data  $T_N = 5.6 \pm 0.1$  K. The inset to fig. 3 shows the same data plotted as  $C_p/T$  vs.  $T^2$ . A linear region is seen between 400 and 900 K $^2$ , which extrapolates to  $\gamma = 18 \text{ mJ/mol K}^2$ . The obtained value should be understood only as a semi-quantitative estimate of the actual electronic coefficient of the specific heat in YbB<sub>2</sub> since, besides the presence of a secondary phase, the temperature region used for the linear fit is rather high. It is inappropriate to use the data below  $T^2 = 400$  K though, where magnetic states begin to strongly influence the measured specific heat.

### 3.4 Resistivity

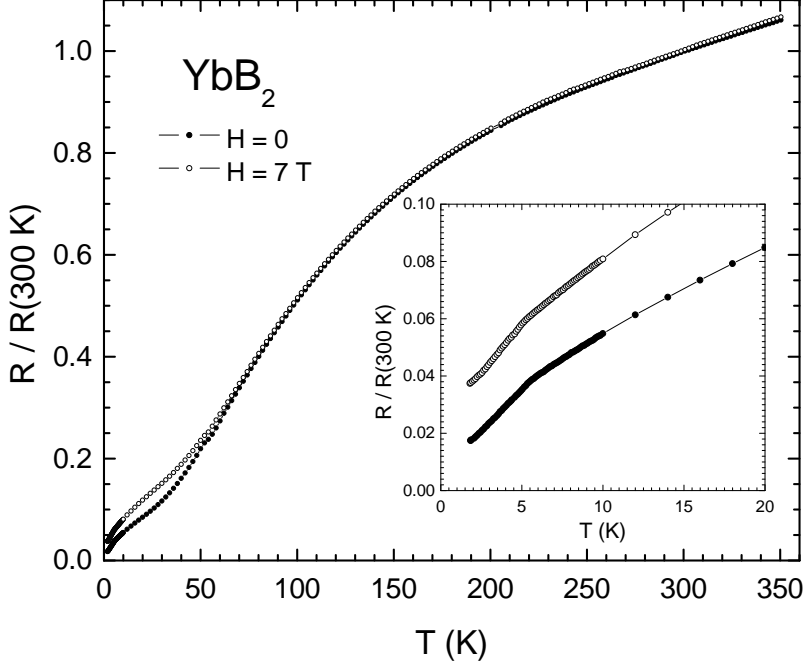


Fig. 4. Temperature dependence of the normalized resistance of a pellet from batch 1300/72, for  $H = 0$  and  $H = 70 \text{ kOe}$ . The inset details the slope change in resistance below 5.6 K and 5.4 K respectively, due to magnetic ordering.

Figure 4 shows resistance data normalized to  $R(300 \text{ K})$ , for zero applied field and for  $H = 70 \text{ kOe}$ . These measurements demonstrate the metallic behavior of  $\text{YbB}_2$ , manifesting a monotonically decreasing resistance as the sample is cooled, and the anti-ferromagnetic ordering is accompanied by a small but abrupt change in slope as the sample is cooled below 5.7 K, detailed in the inset of fig. 4. Analysis of  $dR/dT$  for these curves shows that  $T_N(H = 0) = 5.6 \pm 0.1 \text{ K}$  and  $T_N(H = 70 \text{ kOe}) = 5.4 \pm 0.1 \text{ K}$ , so the suppression of  $T_N$  by an applied field is small.

The broad curvature at intermediate temperatures is a common feature of Yb compounds attributed to CEF effects, since electron scattering is reduced as the upper CEF energy levels become depopulated with cooling. The zero-field residual resistivity ratio, defined here as  $RRR = R(300)/R(1.8)$ , is 57 for sample 1300/72 and grew along the low-pressure synthesis series, starting at  $RRR = 15$  for sample 950/4. This is again consistent with the trends seen in X-Ray diffraction and magnetization, but in the case of transport measurements there is a much greater number of factors that may influence the actual values, such as the conducting properties of each phase as well as the nature/strength

of the intergrain coupling throughout the sample.

## 4 Characterization of samples prepared using the high-pressure synthesis

#### 4.1 X-Ray Powder Diffraction

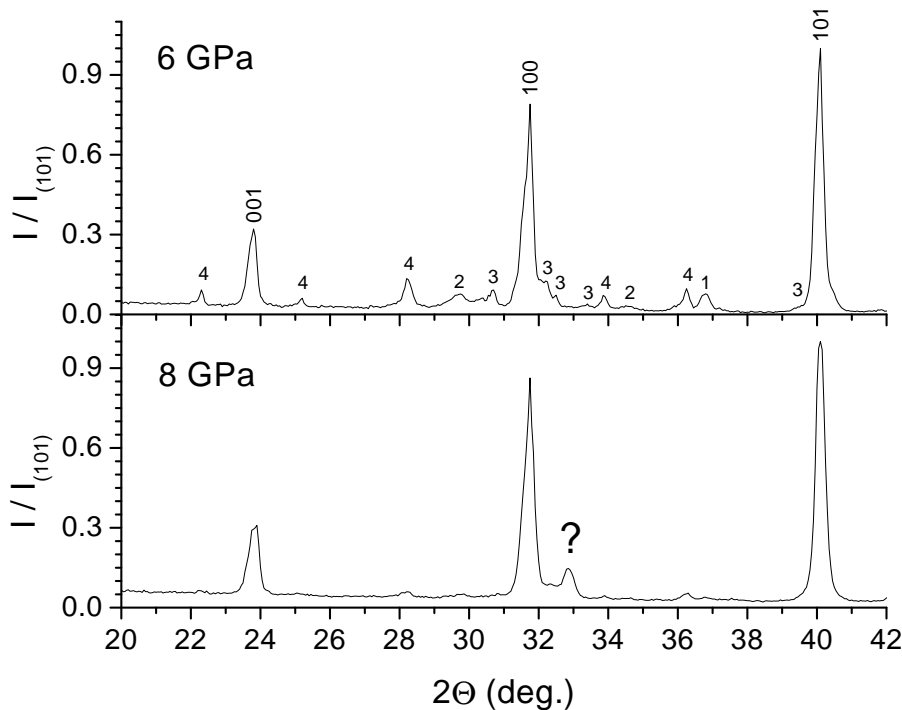


Fig. 5. X-Ray diffraction pattern of  $\text{YbB}_2$  powder from samples 6 GPa and 8 GPa. The 3 major peaks are the  $\text{YbB}_2$  reflections in the shown interval (001,100,101), and the other labels in the top graph mark the peak positions for (1) $\text{YbO}$ , (2)  $\text{Yb}_2\text{O}_3$ , (3) $\text{Yb}_3\text{O}_4$  and (4) $\text{YbB}_4$ .

X-Ray diffraction measurements for the 2 HPS samples are presented in figure 5 for  $20^\circ \leq 2\Theta \leq 42^\circ$ . The top diffractogram, for sample 6 GPa, shows the three expected  $\text{YbB}_2$  reflections in this range, but it is also possible to identify 4 impurity phases: (1) $\text{YbO}$ , (2) $\text{Yb}_2\text{O}_3$ , (3) $\text{Yb}_3\text{O}_4$  and (4) $\text{YbB}_4$ . The sesquioxide  $\text{Yb}_2\text{O}_3$  is the standard result of oxidization of elemental Yb, and it is interesting to note that  $\text{YbO}$  and  $\text{Yb}_3\text{O}_4$  are known to form by reaction of the sesquioxide with Yb at high pressure(15; 16). The presence of the latter two oxide phases indicates that either the starting elemental Yb was partially oxidized, or that there was still some free oxygen gas present during the synthesis procedure. Also, these X-Ray measurements were done about 6 months

after the 6 GPa sample was grown and measured, and it had notably lost much of its cohesion by this time, which may indicate that further oxidization occurred in this period.

The lower diffractogram in fig. 5 is for the 8 GPa sample, and here we observe that the previously identified impurity phases have all but vanished, although by magnifying the noise region it is still possible to detect the secondary phases as being present in very small amounts, most likely not exceeding 5% altogether. However, a new peak has appeared at  $2\Theta = 32.8^\circ$ , which was not observed in any of the previous runs. We were unable to positively associate this peak with any of the more likely candidate phases, such as pure elemental ytterbium and boron, other borides and oxides, or compounds that could possibly result from reaction of the Yb-B melt with NaCl in the pressure cell. But, as will be discussed below, this second phase is very likely a moment bearing one. The refined lattice parameters for  $\text{YbB}_2$  in this sample are  $a = 3.239(3)\text{\AA}$ ,  $c = 3.722(4)\text{\AA}$ .

#### 4.2 DC Magnetization

The magnetization curves of the two HPS samples showed influence of secondary magnetic compounds, among which are  $\text{Yb}_2\text{O}_3$ , known to order anti-ferromagnetically at 2.3 K(17; 18), and  $\text{Yb}_3\text{O}_4$ , reported as weakly paramagnetic(16) but whose magnetic properties are as yet poorly explored. Thus, the beginning of the magnetic ordering of  $\text{YbB}_2$  at 5.7 K is not seen as a peak, but rather as a feature occurring on top of a paramagnetic tail. In fig. 6 we present the low temperature susceptibility behavior of the 8 GPa sample for several fields up to 55 kOe. Applying higher fields to the 8 GPa sample tends to reduce the influence of the underlying paramagnetic tail while showing very little effect on the ordering temperature, and at  $H = 55$  kOe the magnetically ordered region is almost levelled. The inset shows the temperature derivative  $d(\chi T)/dT$  for  $H = 1$  kOe, which gives  $T_N = 4.7 \pm 0.2$  K, a value that is probably artificially low due to the signal from the magnetic secondary phase contaminants.

By fitting the high temperature inverse susceptibility we found  $\mu_{eff} = 4.0$  and  $4.5 \mu_B/\text{YbB}_2$  for the 6 GPa and 8 GPa samples respectively. The deviation from  $4.5 \mu_B/\text{Yb}$  for the 6 GPa sample is easily understood considering the presence of non-magnetic phases such as  $\text{YbO}$ ,  $\text{YbB}_4$  and possibly unreacted Yb. On the other hand, the 8 GPa sample displays the expected effective moment for  $\text{Yb}^{3+}$ . It should be noted that the obtained value cannot be used by itself as a demonstration of the purity of  $\text{YbB}_2$  since, coincidentally,  $\text{Yb}_2\text{O}_3$  has almost exactly the same molecular mass per Yb atom as  $\text{YbB}_2$  (197.04 and 195.04 g/mol(Yb) respectively), but when combined with the X-Ray results it becomes consistent with a much improved phase purity.

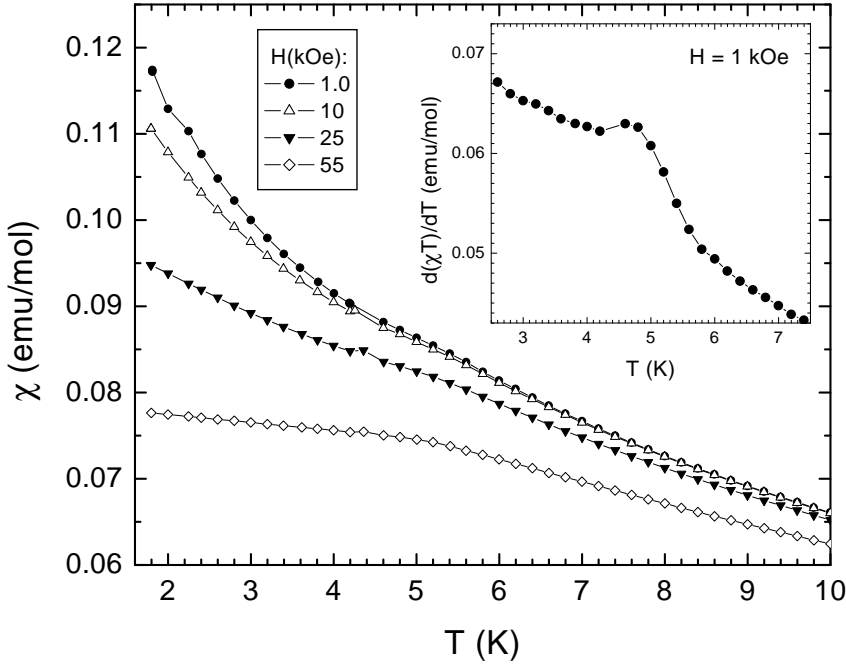


Fig. 6. Temperature dependence of the magnetic susceptibility of sample 8 GPa, in several applied fields. The inset details the peak in  $d(\chi T)/dT$  used to evaluate the ordering temperature.

#### 4.3 Heat Capacity

Figure 7 shows zero-field specific heat data of the 8 GPa sample, taken between 2 K and 40 K. The higher temperature behavior (dominated by the electronic and lattice contributions) is very similar to that observed in fig. 4 for the LPS sample, but as we cool below  $\sim 15$  K the  $C_p$  values of the HPS sample rises much faster, reaching a value of 5.2 J/mol K at the peak, as compared to the 3.0 J/mol K for sample 1300/72. This is qualitatively consistent with the fact that the 8 GPa sample should have a greater mass proportion of  $\text{YbB}_2$ . The feature in  $C_p$  at the ordering temperature is broader in the 8 GPa sample though, so our best estimate is  $T_N = 5.4 \pm 0.2$  K from these data.

The inset shows the same data plotted as  $C_p/T$  vs.  $T^2$ , where the extrapolation of the linear region is between 400 and 900 K $^2$  results in  $\gamma = 14$  mJ/mol K $^2$ , close to the value obtained for sample 1300/72. It is worth noting that these values are significantly larger than those obtained both theoretically and experimentally for many other members of the metal-diboride family(19), and indicates that at least some hybridization of the ytterbium 4f levels with the conduction band electrons may be occurring, with consequent heavy-electron behavior. The study of pressure effects in the specific heat of this compound

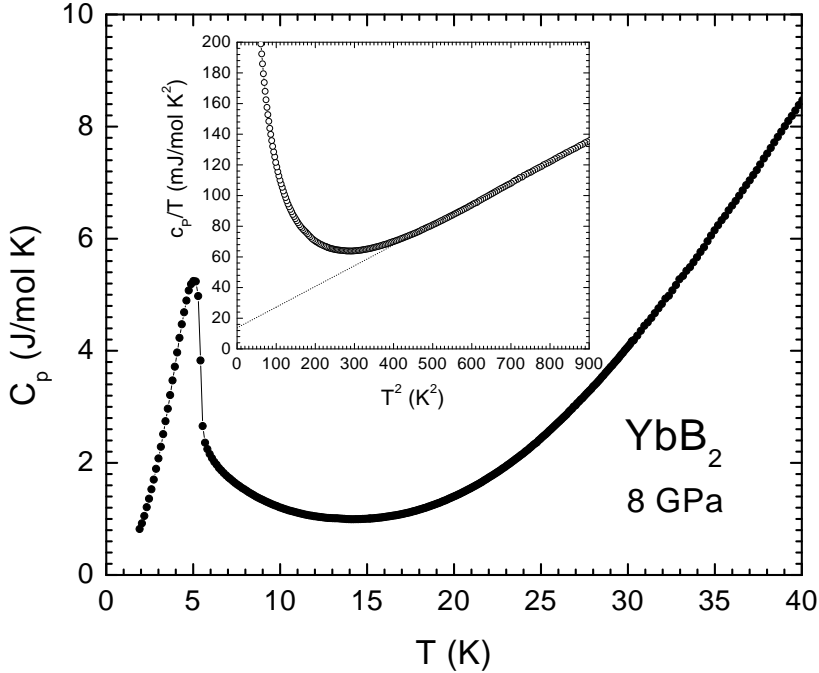


Fig. 7. Temperature dependence of the specific heat of sample 8 GPa. The inset shows the  $T^2$  dependence of  $c_p/T$ , where an estimate of  $\gamma = 14$  mJ/mol K<sup>2</sup> was obtained by linear fitting of the data between 400 and 900 K<sup>2</sup>.

may provide further evidence of such behavior.

#### 4.4 Resistivity

Figure 8 shows zero-field resistance data normalized to  $R(300$  K), for the 6 GPa and 8 GPa samples. The general features observed in the LPS samples are also present here, such as monotonic decrease on cooling, broad curvature at intermediate temperatures, and drop in resistivity at the ordering temperature. The main difference is the almost levelled resistance behavior below  $\sim 30$  K, persisting until the magnetic ordering occurs, at which point resistance begins to drop quite sharply. From a clearly marked discontinuity in  $dR/dT$  we obtain  $T_N = 5.7 \pm 0.1$  K for both samples, although the slope continues to rise until much lower temperatures. The  $RRR$  values obtained for the 6 GPa and 8 GPa samples are only 3 and 5 respectively.

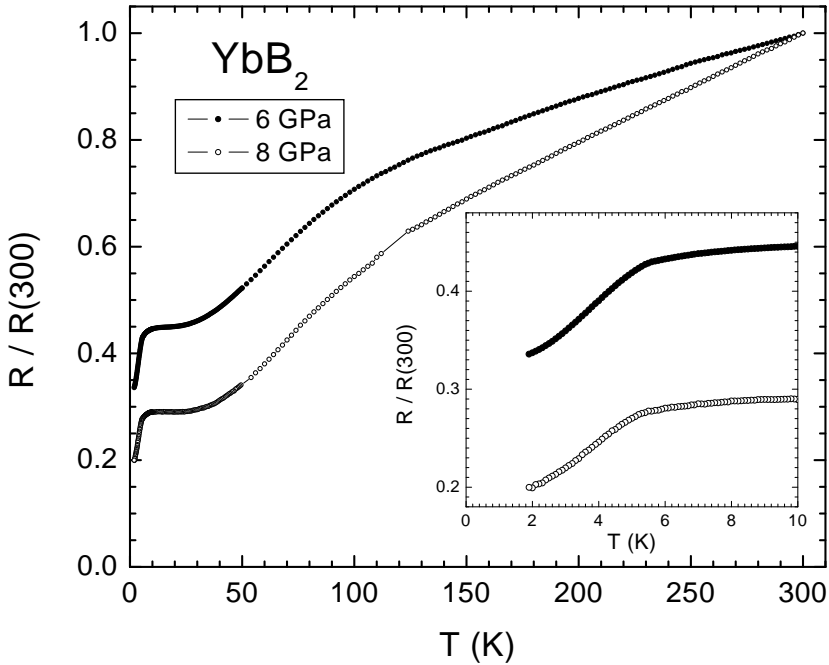


Fig. 8. Temperature dependence of the normalized resistance for samples 6 GPa and 8 GPa. The inset details the drop in resistance below 5.7 K due to magnetic ordering.

## 5 Discussion

We can now compare the results obtained for the LPS and HPS samples. The X-Ray diffractograms allowed us to identify most of the secondary phases present in each sample resultant from these reaction routes. The sample that resulted closest to single-phase  $\text{YbB}_2$  was the one where the elements were melted and recrystallized at 8 GPa. However, this sample contained several different impurity compounds in small quantities, including one that remained unidentified. In contrast, the best sample obtained by the LPS route (1300°C for 72 hours) still contained a significant amount of  $\text{YbB}_4$  as a secondary phase which, however, was the only other compound detectable in the diffractogram.

Magnetization measurements showed that all samples ordered anti-ferromagnetically below 5.7 K regardless of preparation method, with the estimated values from  $d(\chi T)/dT$  being  $T_N = 5.4 \pm 0.2$  K for the 1300/72 sample, and  $T_N = 4.9 \pm 0.2$  K for the 8 GPa sample. This latter value is in disagreement from those obtained by all other experiments, and probably a consequence of interference in the  $d(\chi T)/dT$  analysis by the secondary magnetic phases. The calculated effective moment per Yb atom was closest to its expected value of  $4.5 \mu_B$  for the 8 GPa sample, demonstrating that the Yb atoms are in or very close to

their 3+ state, and the higher phase purity in this sample. However, the fact that the 1300/72 sample contained only a non-magnetic compound as impurity allowed a much clearer observation of the drop in susceptibility resultant from anti-ferromagnetic ordering. Deviations from Curie-Weiss behavior below  $\sim 100$  K were observed in all samples and likely caused by CEF effects on the Yb electronic energy levels.

Specific heat measurements allowed a better precision in the estimation of the ordering temperature for both the 8 GPa and the 1300/72 samples, resulting in  $T_N = 5.4 \pm 0.2$  K and  $T_N = 5.6 \pm 0.1$  K respectively. These samples showed an electronic specific heat coefficient in the range of 14 and 18 mJ/mol K<sup>2</sup> respectively, indicating a possibly enhanced electron mass character of the conduction electrons. Our lack of single-phase samples and of an equivalent non-magnetic compound (such as LuB<sub>2</sub>) to discount the electron/lattice contributions prevents us from attempting any reliable analysis of the magnetic entropy behavior, but it is clear that the 8 GPa sample has accumulated much more magnetic entropy up to the transition temperature.

Resistance measurements showed monotonically decreasing metallic behavior in all samples when cooled from room temperature, including a broad curvature at intermediate temperatures often seen in Yb compounds with CEF splitting. The anti-ferromagnetic ordering was marked as a sudden change in the zero-field resistance slope due to the decrease of spin disorder, at  $T_N = 5.7 \pm 0.1$  K for the HPS samples and  $T_N = 5.6 \pm 0.1$  K for the LPS sample. A small but noticeable decrease to  $T_N = 5.4 \pm 0.1$  K was seen in the resistance measurement at  $H = 70$  kOe for the latter sample. The HPS samples showed much higher electron scattering and lower residual resistivity ratios, possibly due to a greater amount of lattice defects and/or to the influence of non-conducting impurity phases most likely present as grain boundaries. However, one could argue that the better conducting properties of the LPS samples were influenced by the presence in larger proportion of YbB<sub>4</sub> which is known to be metallic(11), and therefore the actual transport behavior of YbB<sub>2</sub> remains to be determined more accurately, if single-phase samples and possibly single crystals are developed in the future.

## 6 Conclusion

In this paper we presented a characterization of some thermodynamic and transport properties of sintered YbB<sub>2</sub> pellets prepared by low-pressure and high-pressure synthesis methods. The two different routes showed several similarities that could be attributed to this compound, but also several relevant differences in sample behavior that arise from the nature and amount of secondary phases. Based on these data we can infer that in YbB<sub>2</sub> the Yb atoms

are essentially in their 3+ state and order magnetically below  $T_N = 5.6 \pm 0.2$  K, which is a high ordering temperature for an Yb-based intermetallic compound. The magnetic ground state is very likely anti-ferromagnetic. We have also obtained indications of CEF effects and enhanced electron mass at the Fermi level. Further development towards obtaining pure, single-phase samples (and if possible in single crystalline form) would be very helpful in corroborating or correcting the results presented here, but the fact that two such different techniques gave robust results gives us some confidence in our basic understanding of the magnetic and electronic properties of  $\text{YbB}_2$ .

Ames Laboratory is operated for the US Department of Energy by Iowa State University under Contract No. W-7405-Eng-82. This work was supported by the Director for Energy Research, Office of Basic Energy Sciences.

## References

- [1] J. Nagamatsu, N. Nakagawa, T. Muranaka, Y. Zenitani, J. Akimitsu, *Nature (London)* 410 (2001) 63.
- [2] K. E. Spear, *J. Less-Common Met.* 47 (1976) 195.
- [3] J. Bauer, *C. R. Hebd. Seances Acad. Sci. Ser. C* 279 (1974) 501.
- [4] J. C. P. Klaasse, W. C. M. Mattens, F. R. D. Boer, P. F. D. Chatel, *Physica B + C* 86-88 (1977) 234.
- [5] A. Svane, W. M. Temmerman, Z. Szotek, L. Petit, P. Strange, H. Winter, *Phys. Rev. B* 62 (2000) 13394.
- [6] Z. Fisk, M. B. Maple, *J. Alloys Compnd.* 183 (1992) 303.
- [7] A. Yatskar, N. K. Budraa, W. P. Beyermann, P. C. Canfield, S. L. Bud'ko, *Phys. Rev. B* 54 (1996) R3772.
- [8] O. Trovarelli, C. Geibel, R. Cardoso, S. Mederle, R. Borth, B. Buschinger, F. M. Grosche, Y. Grin, G. Sparn, F. Steglich, *Phys. Rev. B* 61 (2000) 9467.
- [9] L. G. Khvostantsev, L. F. Vereshchagin, A. P. Novikov, *High Temp. - High Pressures* 9 (1977) 637.
- [10] P. Bonville, P. Imbert, G. Jehanno, F. Gonzalez-Jimenez, *J. Phys. Chem. Solids* 39 (1978) 1273.
- [11] J. Etourneau, J. P. Mercurio, A. Berrada, P. Hagenmuller, R. Georges, R. Bourezg, J. C. Gianduzzo, *J. Less-Common Met.* 67 (1979) 531.
- [12] J. M. Tarascon, J. Etourneau, P. Dordor, P. Hagenmuller, M. Kasaya, J. M. D. Coey, *J. Appl. Phys.* 51 (1980) 574.
- [13] M. E. Fisher, *Philos. Mag.* 7 (1962) 1731.
- [14] P. Bonville, J. A. Hodges, Z. Hossain, R. Nagarajan, S. K. Dhar, L. C. Gupta, E. Alleno, C. Godart, *Eur. Phys. J. B* 11 (1999) 377.
- [15] J. M. Leger, J. Maugrion, L. Albert, J. C. Achard, C. Loriers, C. R. Hebd. *Seances Acad. Sci. Ser. C* 286 (1978) 201.

- [16] J. M. Leger, L. Albert, J. C. Achard, C. Loriers, *Conf. Ser. - Inst. Phys.* 37 (1978) 35.
- [17] R. M. moon, W. C. Koehler, H. R. Child, L. J. Raubenheimer, *Phys. Rev.* 176 (1968) 722.
- [18] H. Li, C. Y. Wu, J. C. Ho, *Phys. Rev. B* 49 (1994) 1447.
- [19] P. Vajeeston, P. Ravindran, C. Ravi, R. Asokamani, *Phys. Rev. B* 63 (2001) 045115.